Available online at www.sciencedirect.com
ScienceDirect
Journal of the European Ceramic Society 27 (2007) 1443–1448
www.elsevier.com/locate/jeurceramsoc

Threshold strength evaluation on an Al_2O_3–ZrO_2 multilayered system

R. Bermejo [a], Y. Torres [a], C. Baudín [b], A.J. Sánchez-Herencia [b], J. Pascual [c], M. Anglada [a], L. Llanes [a,*]

[a] *Departamento de Ciencia de Materiales e Ingeniería Metalúrgica, Universidad Politécnica de Cataluña, Avda. Diagonal 647 (ETSEIB), 08028 Barcelona, Spain*
[b] *Instituto de Cerámica y Vidrio (CSIC), C/Kelsen 5, 28010 Madrid, Spain*
[c] *Institut für Struktur- und Funktionskeramik der Montanuniversität Leoben, Peter-Tunner-Strasse 5, 8700 Leoben, Austria*

Available online 15 June 2006

Abstract

The fracture behaviour of an alumina–zirconia multilayered ceramic obtained by slip casting has been evaluated and compared to monolithic alumina taken as a reference. It is found that the laminated system exhibits an apparent fracture toughness $K_{apt,c}$, calculated experimentally (SEPB) and analytically with a weight function approach, higher than twice the value determined for the monolithic material. Additionally, the experimental rupture tests accomplished indicate the existence of a threshold strength in the multilayer. The increase in $K_{apt,c}$ in the laminate, associated with a pronounced *R*-curve behaviour, is discussed in terms of the high compressive stresses in the internal layers and their effect on the effective driving force for crack extension.

Keywords: Slip casting; Composites; Mechanical properties; Toughness

1. Introduction

In the last decades, new microstructural design concepts have been attempted for improving fracture toughness of structural ceramics. Among them, doping, fibre and/or particle reinforcement, functional grading and layered architectural design may be highlighted. In particular, ceramic composites with a layered structure such as alumina–zirconia[1–3] and mullite-alumina[4] among others, have been reported to exhibit an increased apparent fracture toughness and energy absorption as well as non-catastrophic failure behaviour. For strongly bonded multilayers the elastic mismatch during sintering between adjacent layers, resulting from the difference in Young's moduli, thermal expansion coefficients, chemical reactions and/or phase transformations, generates residual stresses throughout the material. These residual stresses can be controlled in order to improve their mechanical properties. On ceramics and glasses, for instance, the compressive stresses on the surface have proven to be useful for increasing their fracture strength.[1,5] On the other hand, laminar ceramics designed with compressive stresses in the bulk may present a threshold strength below which catastrophic failure does not occur. Such a scenario has been reported by Rao et al.[6] for an alumina–alumina mullite multilayered system when a tensile stress was applied parallel to the layers. From this perspective, zirconia-containing laminar ceramics have been employed to develop compressive stresses in the internal layers by means of the tetragonal to monoclinic phase transformation that takes place when cooling down during sintering.[1,7] The corresponding volume increase associated with such transformation will condition the residual stress field within the multilayer. Under certain conditions, these compressive stresses may act as a barrier to crack propagation. In other cases, crack bifurcation and/or deflection phenomena result in an increase of the material fracture toughness and energy absorption capability.[8]

It is the purpose of this investigation to evaluate the fracture behaviour of an alumina/zirconia-based multilayered ceramic, with highly compressed thin layers, in comparison to the alumina monolith taken as reference material. In doing so, special attention is paid to evaluate the possible existence of a threshold strength under flexural loading normal to the layer plane. Apparent fracture toughness is experimentally determined using the SEPB method and the *R*-curve behaviour evaluated analytically by the weight function approach. Finally, work of fracture is estimated by conducting crack opening displacement (COD) tests on notched laminated samples.

* Corresponding author. Tel.: +34 934011083; fax: +34 934016706.
E-mail address: luis.miguel.llanes@upc.edu (L. Llanes).

0955-2219/$ – see front matter © 2006 Elsevier Ltd. All rights reserved.
doi:10.1016/j.jeurceramsoc.2006.05.037

2. Experimental work

2.1. Material processing and basic characterization

Laminar ceramic composites have been fabricated via sequential slip casting. Starting powders were submicron-sized Alumina HPA 0.5 (Condea, USA) with a particle size of 0.25 μm and pure zirconia TZ-0 (Tosoh, Japan) with a particle size of 0.3 μm. Slurries were made by mixing starting powders with DI water that contained the desired amount of dispersant used for stabilization. A slurry composed of Al_2O_3/5 vol.% Y_2O_3-stabilized ZrO_2 (t-ZrO_2), referred as ATZ, was used to form the thicker layers. The t-ZrO_2 was employed to control the grain size of the Al_2O_3 during densification. In order to form the thin layers a slurry containing Al_2O_3/30 vol.% ZrO_2 (m-ZrO_2), noted as AMZ, was utilized. Details of the processing procedure may be found in a previous report.[9] Cast specimens were then fired at 1550 °C for 2 h with a heating and cooling rate of 5 °C/min. Rectangular plates of approximately 60 mm × 60 mm × 4 mm were obtained. Flexural bars were cut from the plates, and the top and lateral surfaces of each specimen were polished to a 3-μm finish with a diamond abrasive for microstructural observation and mechanical characterization. A homogeneous layer thickness was obtained for both ATZ and AMZ layers, resulting in a symmetrical multilayered architecture (see Fig. 1).

2.2. Residual stress estimation

Dynamic sintering was carried out on the monoliths to calculate the residual stresses generated in the laminate system. Transformation strains of the thin layers containing monoclinic ZrO_2 were estimated by measuring the transformation strains of monolithic bar specimens with the same compositions as the thin compressive layers. The dilatational strains produced by these dense AMZ and ATZ monoliths, during cooling from densification temperature, were measured with a dilatometer (DIL 402 E/7, Netzsch, Germany). The residual stress profile throughout the multilayer was determined by a 3D finite element model developed elsewhere.[10] All materials were assumed to be isotropic so that only two independent properties such as the Young's modulus and the Poisson's ratio had to be provided. Thermal expansion coefficients ($\alpha_{ATZ} = 9.82 \times 10^{-6}\ K^{-1}$ and $\alpha_{AMZ} = 8.02 \times 10^{-6}\ K^{-1}$) were discretely introduced in the model from data corresponding to the dilatometry curves, considering 1200 °C as the reference temperature.

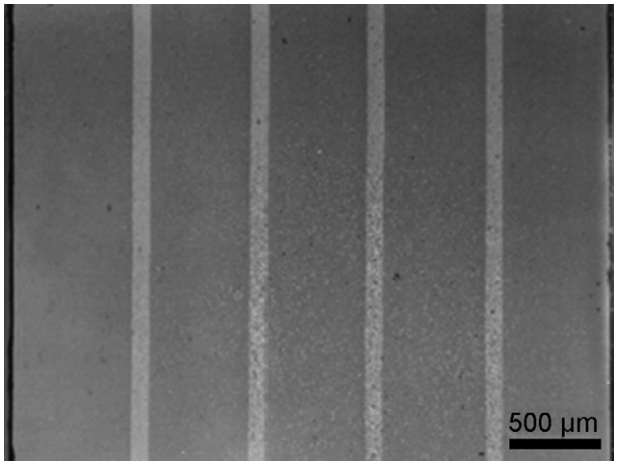

Fig. 1. SEM micrograph of the Al_2O_3–ZrO_2 multilayered architecture obtained by slip casting.

2.3. Threshold strength evaluation

Laminar ceramics with high compressive residual stresses on the inner layers may exhibit an apparent *R*-curve behaviour[11] as well as a threshold strength, regardless of the type and size of initial flaws. In order to estimate and study the effect of a possible presence of threshold strength on the mechanical behaviour of the laminate investigated, four specimens were ground and polished up to 3 μm at the surface and at one of the lateral faces. Different combinations of Vickers indentations were placed longitudinally on each specimen surface with an offset separation distance of 2 mm to avoid any crack interaction: (a) 200, 200, 100, 50 N; (b) 150, 150, 100, 50 N; (c) 100, 100, 50, 30 N; (d) 50, 50, 30, 30 N. The same procedure was conducted on the ATZ monoliths for comparison. The crack length was measured by means of an optical microscope and by recourse to Nomarski interference contrast. Then, all the specimens were tested until fracture under four-point bending on a servo-hydraulic machine, with inner and outer spans of 10 and 20 mm, respectively, at a load rate of 100 N/s. The failure stress for the indented specimens, σ_{Ri}, was calculated using Eq. (1):

$$\sigma_{i,y} = \frac{E_i M}{(EI)}(y - y_{na}) \quad (1)$$

where E_i is the Young's modulus of the corresponding layer, M the moment for the case of four-point bending tests ($M = Fa$, where F is the applied load and a the distance between inner and outer spans), y_{na} is the position of the neutral axis and EI the flexural rigidity of the composite calculated for bending perpendicular to the layers.[12,13]

2.4. Fracture toughness assessment

In the case of the monolithic materials, fracture toughness was evaluated by two different methods: (i) the microfracture indentation (IM) method, proposed by Anstis et al.[14] and (ii) the single-edge V-notch beam (SEVNB) method.[15] For the latter, a razor blade automatic machine was utilized to create the notch, which was sharpened up to a radius of less than 10 μm to minimize the influence of notch radius on K_{Ic}.[16] This method was also employed for the evaluation of the fracture toughness on the laminates. In doing so, a notch of the same depth and radius as that for the monolith was machined in the outer most ATZ layer. Very interesting, after reaching a certain notch depth a straight, thin, through-thickness crack developed from the notch and arrested at the ATZ/AMZ interface (see Fig. 2a), yielding as a result an effective SEPB configuration. Within this context, and considering that when fracture occurs the crack continues in mode I (see Fig. 2b), it is sustained to employ the expression

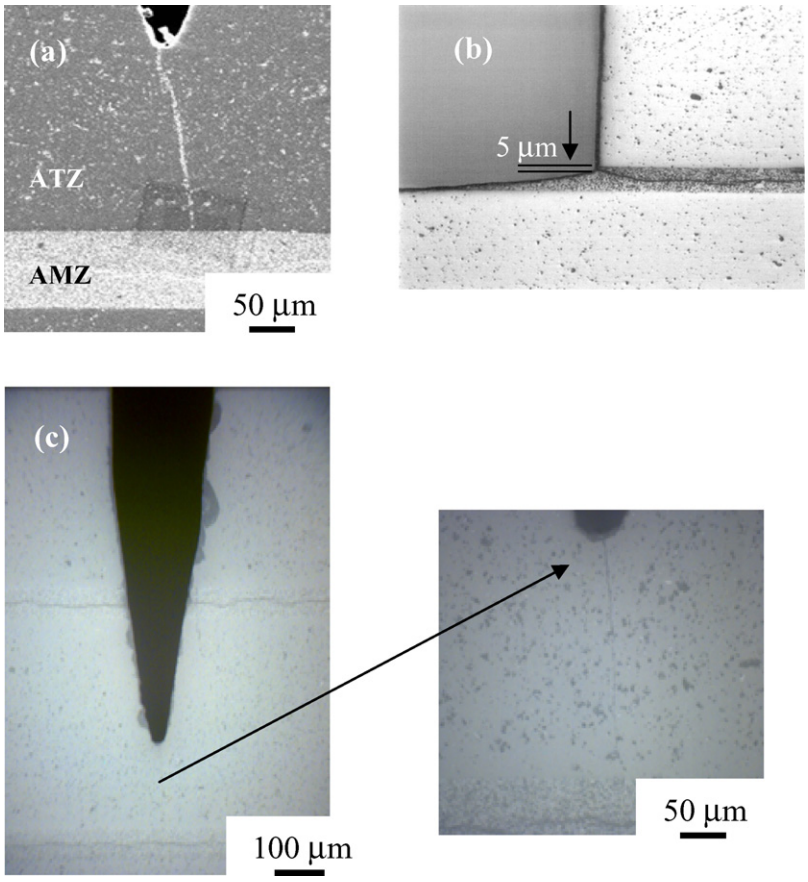

Fig. 2. (a) SEM micrograph showing a straight, fine crack that arises from the notch and arrests at the first ATZ/AMZ interlayer; (b) the crack continues propagating in mode I a certain distance before bifurcation; (c) a second notch is made entering the second ATZ layer, where a crack also appears from the notch and stops at the second ATZ/AMZ layer.

given by Tada et al.[17] to determine the apparent fracture toughness, K_{Ia}, at the first ATZ/AMZ interlayer. Following the same procedure, another value of the apparent fracture toughness of the laminate, K_{Ib}, was determined by generating a notch entering the second ATZ layer (see Fig. 2c) where, once again, a crack of the same characteristics as above arose from the notch and stopped at the second ATZ/AMZ interface.

In addition, a fracture mechanics weight function analysis was effectively used to estimate the crack growth resistance behaviour (*R*-curve) as a function of the position of an edge crack within each multilayered system investigated. The so called apparent fracture toughness $K_{apt,c}$ (since it is influenced by the residual stresses) for an arbitrary stress distribution $\sigma_{res}(x)$ normal to the layer plane, may be defined as follows:

$$K_{apt,c} = K_{Ic} - \int_0^a h(a, x)\sigma_{res}(x)\,dx \quad (2)$$

where K_{Ic} is the intrinsic fracture toughness of each individual layer calculated by the SEVNB method in the corresponding monoliths, x the distance along the crack length measured from the surface, a the crack length, and $h(a, x)$ is a weight function as developed by Fett and Munz for an edge crack in a bar,[18] commonly employed in the evaluation of *R*-curve behaviour for multilayered systems.[19–21]

2.5. Work of fracture: COD tests

To determine the work of fracture in the laminate in comparison with that of the ATZ monolith, samples were tested in three-point bend under crack opening displacement (COD) control at a rate of 1 μm/s. Identical specimens for monoliths and laminates were notched using a razor blade automatic machine. Notches were machined to enter a small depth into the ATZ phase to avoid the appearance of a crack out of the notch tip for the case of the laminates, as described above. Thus, depths of 150 μm were not surpassed in any case. A COD-gauge was attached to the specimen surface at the notch site to register the crack opening displacement. Additionally, the extension of the crack in the SEVNB specimens was continuously monitored using a long distance focal optical microscope (Questar QM100) with a final magnification of 1000×. Crack opening displacement and load data were recorded by a software (Labview 6.1) coupled to the testing set-up.

Assuming that all the work done is consumed in the growth of the crack and no significant elastic energy is stored in the specimen during testing, the total fracture energy may be attempted through integration of the registered load–COD curve/material volume unit for the ATZ monolith and for the laminate.[22]

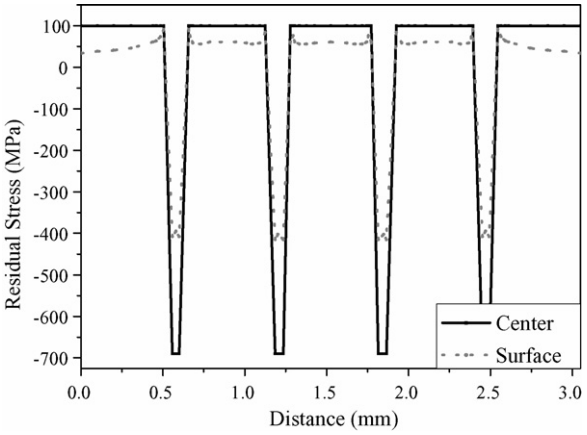

Fig. 3. Stress distribution through the layers in the bulk and at the surface of the multilayer, calculated using a 3D finite element model.

3. Results and discussion

3.1. Residual stress distribution

Fig. 3 represents the magnitude and distribution profile of the residual stresses within the inner and outer layers of the laminate calculated both at the surface and in the bulk of the specimen, using a 3D finite element model. Compressive stresses seem to present a constant value of −690 MPa through the entire thin layer. For the internal ATZ layers a symmetrical distribution is obtained reaching a maximum value of 100 MPa at the ATZ/AMZ interfaces. On the other hand, for the outer layers residual stresses decrease near the free surface. These results are in good agreement with those reported on a previous work where residual stress distribution was evaluated by the indentation technique and analytical solutions.[9]

3.2. Threshold strength

Fig. 4 represents the variation of the failure stress with the square root of the initial flaw size, c, for the indented ATZ monolith and for the laminate investigated. From these results,

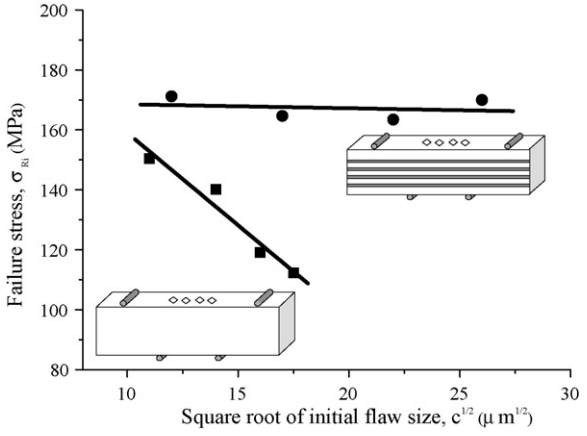

Fig. 4. Plot of measured four-point bending failure stress vs. square root of crack length in ATZ monolith (■) and laminate (●) specimens containing several groups of Vickers indentations at the surface.

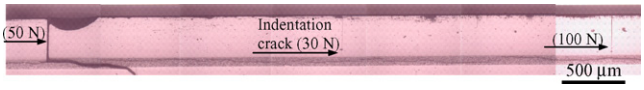

Fig. 5. Optical micrograph showing the failure of the laminate (indentation load of 50 N) when the threshold stress is reached. The rest of indentation cracks corresponding to different loads placed at the ATZ surface have become through-thickness cracks and arrested at the AMZ/ATZ interface.

several conclusions may be inferred: (i) for the same indentation loads, measured crack lengths are always larger for the laminate, corroborating the presence of tensile residual stresses in the indented ATZ layer, as reported in Fig. 3, (ii) the failure stress values are higher for the laminate for every indentation flaw size, pointing out the enhanced mechanical behaviour in comparison to the ATZ monolith, (iii) the constant value of these failure stresses, regardless of the indentation flaw size, allows to indicate the existence of a threshold strength in the laminate with a value of 167 ± 4 MPa, and (iv) fracture of the ATZ monolith always occurs from the defect originated by the largest indentation load, as it should be expected. However, in the multilayered material fracture takes place randomly from any of the indentations performed. This may be explained by the fact that, regardless of the indentation load applied in the laminate, the crack shape, a/c, is initially always greater than one, and rises when an external load is applied (as demonstrated experimentally by grinding and polishing procedures), helped by the tensile residual stresses in the ATZ layer, more significant as the interface is approached (Fig. 3). When a is equal to the ATZ layer thickness the crack stops, and then c starts to grow until the crack becomes a through-thickness one. Once that all the indentation cracks have become through-thickness cracks and arrested at the AMZ layer (Fig. 5), the stress intensity factor in any of them is equivalent, regardless of the indentation load used for inducing them.

3.3. Fracture toughness

Fracture toughness for the monolithic materials evaluated by the microfracture indentation (IM) and the single-edge V-notch beam (SEVNB) methods are reported in Table 1. It is interesting to note here that these K_{Ic} values may be even overestimated because the IM method is affected by the residual stress field inherent to the indentation, while the notch radius for the SEVNB method is not as sharp as a real crack and is greater than the microstructure scale length.

As a comparison, the apparent fracture toughness, K_{Ia} and K_{Ib}, for the multilayered material were 7.1 and 8.1 MPa m$^{1/2}$, as determined at the first and second AMZ layer, respectively.

Table 1
Fracture toughness values for the ATZ and AMZ monoliths as determined by means of the IM and SEVNB methods

Material	K_{Ic} (MPa m$^{1/2}$)	
	IM	SEVNB
ATZ	3.5	3.2
AMZ	2.9	2.6

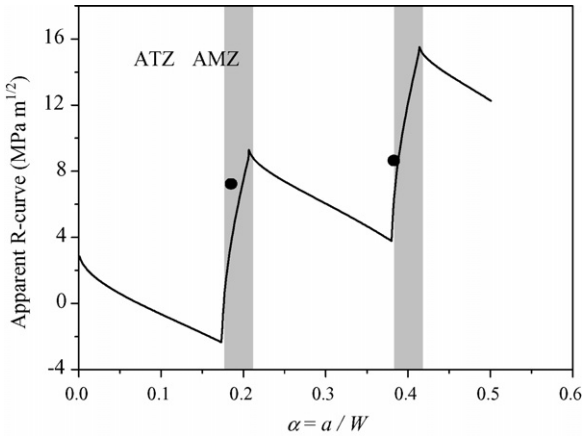

Fig. 6. Apparent fracture toughness calculated analytically using the weight function approach, taking into account the contribution of the residual stresses through the laminate.

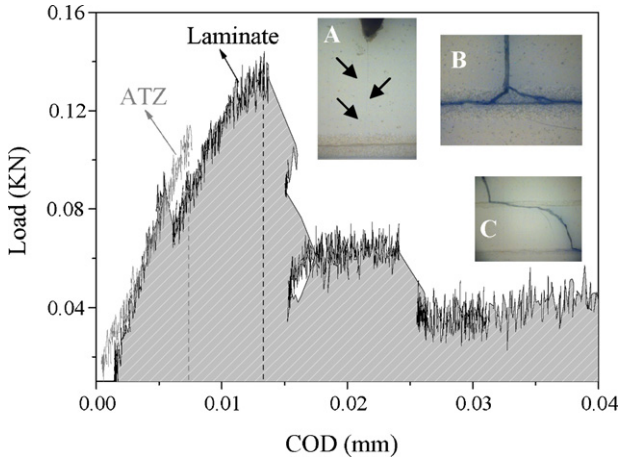

Fig. 7. Load-COD curves for *ATZ* monolithic and *laminate* notched specimens at a COD rate of 1 μm/s. Maximum load for the ATZ corresponds to the crack initiation and consequent fracture of the specimen. For the case of the laminate, although the first drop in load is also related to crack initiation, crack is arrested at the first ATZ/AMZ interface (see micrograph A) and an increase in load is required to continue with the crack propagation (see micrograph B). Crack bifurcation and crack deflection can be observed in the fractured specimens (see micrographs B and C). Shaded area shows the higher work of fracture of the laminate in comparison to the ATZ monolith.

On the other hand, the apparent fracture toughness, $K_{apt,c}$, determined analytically for the first layers using the weight function method, is presented in Fig. 6, showing the *R*-curve behaviour of this multilayered system. It can be inferred that $K_{apt,c}$ decreases while the crack propagates through the ATZ tensile layers. However, there is a significant *R*-curve raise when entering a highly compressed AMZ layer, which is the responsible for the crack arrest and the subsequent threshold effect. The negative values for $K_{apt,c}$ may be explained by the relatively high residual tensile stresses present in the ATZ layers. This might also be associated with the spontaneous cracks arising from the notches at some point within the ATZ tensile phase, as discussed in Section 2.

The experimental values for apparent fracture toughness of the laminate are in fair agreement with those predicted by the analytical model, yet more tests should be conducted to better evaluate the *R*-curve effect in this material.

3.4. Fracture energy

The COD tests performed on ATZ monoliths and laminates allowed to evaluate the work required to break the samples. In the case of the monolith, the fracture initiated at the notch tip when reaching a certain crack opening displacement. Failure was catastrophic as it corresponds to a brittle material. On the other hand, failure in the laminate originated also at the notch tip but for a smaller stress value (see Fig. 7). It can be inferred from the recorded data that the first drop in load occurred at a load value below the maximum load reached by the monolithic sample. This difference is explained by the fact that tensile stresses are present in the laminate at the notch site increasing the stress intensity factor at that point. Nevertheless, the crack initiated at the notch tip does not produce catastrophic failure as in the case of the monolith, since it arrests at the first ATZ/AMZ interface (see Fig. 7A). To maintain the crack opening displacement rate during the test a further increase in load is required. When the crack enters the first ATZ/AMZ interface, which corresponds to the maximum load in the load/COD curve, a second drop in load is observed. This effect is repeated any time the crack faces a new ATZ/AMZ interface (see Fig. 7).

The total fracture energy, *G*, for the ATZ monolith and for the laminate was evaluated through integration of the load–COD registered curve/material volume unit (Fig. 7) resulting in values of 29 and 178 J/m^2, respectively. In particular, the area of the curve associated with the first ATZ/AMZ interface is of 123 J/m^2, which is in good agreement with the value for the fracture energy estimated from the experimental fracture toughness at the first interface (G_{Ia} = 128 J/m^2; for K_{Ia} = 7.1 MPa m$^{1/2}$, E = 373 GPa and υ = 0.22).

The enhanced fracture behaviour of the multilayer investigated in comparison with the ATZ monolith is due to the compressive stresses in the thin AMZ layers, which depend on the thickness ratio of the layers. In this particular case, crack bifurcation (Fig. 7B) and crack deflection (Fig. 7C) are observed. As a consequence, a step-wise behaviour at the fracture surface of the laminate is observed, as compared to the flat character exhibited by the ATZ monolith. The existence of these mechanisms depend, for a given layer thickness ratio, on the AMZ layer thickness, being possible their absence for very thin layers. Further studies are in progress on this kind of multilayers with various layer thickness ratios to study its effect on the threshold strength and crack propagation mechanisms.

4. Conclusions

The fracture behaviour of an Al_2O_3/ZrO_2 multilayered material has been characterized and compared to that of a monolithic alumina, taken as reference. From the results, the following conclusions can be drawn:

(i) The residual stresses developed in the multilayer during sintering reveal a difference in magnitude and distribution between external and internal ATZ layers. For the former, residual stresses decrease near the free surface. For the latter a symmetrical distribution is observed, reaching a maximum value close to the ATZ/AMZ interfaces. In the bulk, the mean value of these tensile residual stresses is over 100 MPa whilst for the compressive layers reaches a maximum of −690 MPa.

(ii) In the multilayered material investigated a threshold strength of 167 ± 4 MPa is encountered for monotonic loads applied normal to the layer plane, regardless of the initial flaw size. This behaviour is contrary to the ATZ monolith where the failure stress diminishes with the flaw size.

(iii) The fracture toughness of the ATZ monolith (SEVNB) and laminate is of 3.2 and 7.1 MPa $m^{1/2}$, respectively. The apparent fracture toughness of the laminate structure determined experimentally with the SEPB method is in fair agreement with the values predicted by the weight function analytical procedure.

(iv) The fracture energy of the laminated composite is about six times higher than that of the monolithic alumina. The mechanism responsible for energy dissipation is the bifurcation and/or deflection of cracks when they enter the thin compressive layers showing a step-wise fracture in comparison with the flat character encountered for most of the brittle materials.

These results indicate that this multilayered structure design may be effective for improving the resistance to crack propagation as well as enhancing the reliability of structural ceramic components due to the presence of a threshold strength under loading axis normal to the layer plane.

Acknowledgments

Work supported by the Spanish Ministry of Science and Technology, through grant MAT-2002-00368. Some of the authors RB and JP acknowledge the financial support provided through the European Community's Human Potential Programme under contract HPRN-CT-2002-00203, [SICMAC].

References

1. Virkar, A. V., Huang, J. L. and Cutler, R. A., Strengthening of oxide ceramics by transformation-induced stresses. *J. Am. Ceram. Soc.*, 1987, **70**, 164–170.
2. Requena, J., Moreno, R. and Moya, J. S., Alumina and alumina/zirconia multilayer composites by slip casting. *J. Am. Ceram. Soc.*, 1989, **72**, 1511–1513.
3. Marshall, D. B., Ratto, J. J. and Lange, F. F., Enhanced fracture toughness in layered microcomposites of Ce-ZrO_2 and Al_2O_3. *J. Am. Ceram. Soc.*, 1991, **74**, 2979–2987.
4. Katsuki, H. and Hirata, Y., Coat of alumina sheet with needle-like mullite. *J. Ceram. Soc. Jpn.*, 1990, **98**, 1114–1119.
5. Green, D. J., Tandon, R. and Sglavo, V. M., Crack arrest and multiple cracking in glass through the use of designed residual stress profiles. *Science*, 1999, **283**, 1295–1297.
6. Rao, M. P., Sánchez-Herencia, A. J., Beltz, G. E., McMeeking, R. M. and Lange, F. F., Laminar ceramics that exhibit a threshold strength. *Science*, 1999, **286**, 102–105.
7. Sanchez-Herencia, A. J., Pascual, C., He, J. and Lange, F. F., ZrO_2/ZrO_2 layered composites for crack bifurcation. *J. Am. Ceram. Soc.*, 1999, **82**, 1512–1518.
8. Clegg, W. J., Kendall, K., Alford, N. M., Button, T. W. and Birchall, J. D., A simple way to make tough ceramics. *Nature*, 1990, **347**, 455–461.
9. Bermejo, R., Torres, Y., Sánchez-Herencia, A. J., Baudín, C., Anglada, M. and Llanes, L., Fracture behaviour of an Al_2O_3–ZrO_2 multilayered ceramic with residual stresses due to phase transformations. *Fatigue Fract. Eng. Mater. Struct.*, 2006, **29**, 71–78.
10. Bermejo, R., Llanes, L., Anglada, M., Supancic, P. and Lube, T., Thermal shock behavior of an Al_2O_3/ZrO_2 multilayered ceramic with residual stresses due to phase transformations. *Key Eng. Mater.*, 2005, **290**, 191–198.
11. Fett, T. and Munz, D., Evaluation of *R*-curve effects in ceramics. *J. Mater. Sci.*, 1993, **28**, 742–752.
12. Gere, J. M. and Timoshenko, S. P., *Mechanics of Materials*. Stanley Thornes Ltd., UK, 1999, pp. 391–404.
13. Malzbender, J. and Steinbrech, R. W., Mechanical properties of coated materials and multi-layered composites determined using bending methods. *Surf. Coat. Technol.*, 2004, **176**, 165–172.
14. Anstis, G. R., Chantikul, P., Lawn, B. R. and Marshall, D. B., A critical evaluation of indentation techniques for measuring fracture toughness. I. Direct crack measurements. *J. Am. Ceram. Soc.*, 1981, **64**, 533–538.
15. Kuebler, J., Fracture toughness of ceramics using the SEVNB method; from a preliminary study to a standardized method. *Fracture Resistance Testing of Monolithic and Composite Brittle Materials, ASTM STP 1409*. American Society for Testing and Materials, West Conshohocken, PA, USA, 2002.
16. Damani, R., Gstrein, R. and Danzer, R., Critical notch-root radius effect in SENB-S fracture toughness testing. *J. Eur. Ceram. Soc.*, 1996, **16**, 695–702.
17. Tada, H., Paris, P. C. and Irwin, G. R., *The Stress Analysis of Cracks Handbook*. Paris Productions Incorporated (and Del Research Corporation), St. Louis, USA, 1973, pp. 2.13–2.15.
18. Fett, T. and Munz, D., *Stress Intensity Factor and Weight Functions*. Computational Mechanics Publications, Elsevier, Southampton, UK, 1997, p. 408.
19. Rao, M. P., Rödel, J. and Lange, F. F., Residual stress induced *R*-curves in laminar ceramics that exhibit a threshold strength. *J. Am. Ceram. Soc.*, 2001, **84**, 2722–2724.
20. Moon, R., Hoffman, M., Bowman, J. H., Trumble, K. and Rödel, J., A weight function analysis on the *R*-curve behaviour of multilayered alumina-zirconia composites. *J. Am. Ceram. Soc.*, 2002, **85**, 1505–1511.
21. Lugovy, M., Slyunyayev, V., Orlovskaya, N., Blugan, G., Kuebler, J. and Lewis, M., Apparent fracture toughness of Si_3N_4-based laminates with residual compressive or tensile stresses in surface layers. *Acta Mater.*, 2005, **53**, 289–296.
22. Tattersall, H. G. and Tappin, G., The work of fracture and its measurements in metals, ceramics and other materials. *J. Mater. Sci.*, 1966, **1**, 296–301.